J Mater Sci (2008) 43:3881–3888
DOI 10.1007/s10853-007-2158-9

Geometrical and physical models of martensitic transformations in ferrous alloys

Robert C. Pond · Xiao Ma · John P. Hirth

Received: 18 July 2007 / Accepted: 10 September 2007 / Published online: 6 March 2008

Abstract The classical theory of the crystallography of martensitic transformations developed in the 1950s is based on the notion that the interface between the parent and product phases is an invariant plane of the shape deformation. Underlying this hypothesis is the expectation that such interfaces do not exhibit long-range strain, and the geometric theory is an algorithm for finding invariant planes, the orientation relationship and transformation displacement. In the context of ferrous alloys, the classical theory has been applied successfully to transformations with {295} habit planes, but is less satisfactory for {575} for example. A new model of martensitic transformations has been presented recently based on dislocation theory, incorporating developments in the understanding of the topological properties of interfacial defects. Topological arguments show that glissile motion of transformation dislocations, or disconnections, can only occur in coherent interphase interfaces. Hence, the interface in the model comprises coherent terraces with a superimposed network of disconnections and crystal dislocations. It is demonstrated explicitly that this defect network accommodates the coherency strains, and that lateral motion of the disconnections across the interface effects transformation in a diffusionless manner. Moreover, it is shown that a broader range of habit planes is predicted on the basis of the semi-coherent interface model than the invariant plane notion. In the case of ferrous alloys, it will be shown that a range of viable solutions arise which include {575}.

R. C. Pond (✉) · X. Ma
Department of Engineering, University of Liverpool,
P.O. Box 147, Liverpool L69 3BX, UK
e-mail: r.c.pond@liv.ac.uk

J. P. Hirth
114 E. Ramsey Canyon Rd., Hereford, AZ 85615, USA

Introduction

Martensitic transformations are diffusionless and displacive [1]. They occur with isothermal, athermal or burst kinetics; in most cases, nucleation is thought to be thermally activated, and growth is not a rate-limiting process except for slow isothermal instances [2]. The structure of the parent–martensite interface is a key issue in all these considerations, and the object of the present article is to review recent progress in the development of a model of the interface based on dislocation theory. In the phenomenological model, developed by Wechsler et al. [3] and Bowles and MacKenzie [4], the interface is envisaged as an invariant plane of the shape transformation. This notion is consistent with a large number of experimental observations at the resolution of the optical microscope, although certain martensitic morphologies, in Fe alloys for example, are exceptions [5]. A dislocation model can elucidate the structure of interfaces at the atomic level and could therefore resolve the inapplicability of the classical model to certain transformations. Furthermore, dislocation modelling should relate directly to kinetic issues. In the following sections, the dislocation model, referred to as the topological model (TM) [6, 7], is outlined and compared with the phenomenological model of martensite crystallography (PTMC). The TM is then applied to the cases of the β to α transformation in Ti and γ to α in Fe-based alloys.

Topological model of martensitic interfaces

The ideal parent–martensite interface is required to be glissile, i.e. to migrate readily without long-range diffusion, and in a manner that produces the transformation shear. In addition, unit cells of the two phases should only be distorted in the vicinity of the interface. The former

property can arise through the motion across an interface of transformation dislocations, or disconnections [8], i.e. line defects with both dislocation and step character. The latter property is characteristic of semicoherent interface structures [9]; in general, at least two sets of dislocations are needed to accommodate coherency strains. Thus in the simplest case, the TM envisages one array of disconnections and one of crystal defects, slip or twinning, as depicted schematically in Fig. 1, which is similar to structures proposed in earlier works [10–13]. More generally, there can be more than one set of defects in the latter array. Synchronous motion of the disconnection array across the interface can, in special crystallographic circumstances, produce a martensitic transformation. We now enumerate these special circumstances.

Glissile motion of disconnections only arises in particular interphase interfaces; the number of atoms must be conserved during motion, but not necessarily the volume occupied since the densities of the two phases are different in general [14]. Certain disconnections with appropriate Burgers vector and step height couples, (**b**, h), can move conservatively across *coherent* interfaces, enabling a "military" transfer of material from one crystal to the other, particularly where atomic shuffling is minimal [15]. Thus, the starting point of the TM is to identify candidate terraces where low-index planes of the two phases abut with modest coherency strain. The (**b**, h) of disconnections that are glissile in this coherently strained reference state can be identified using the topological theory of interfacial defects [16]. It is also necessary to select the second set of defects so that intersection nodes with the disconnections are not sessile. Slip or twinning defects (**b**, 0) from the martensite fulfil this role, provided they are able to glide to the interface [17]; such defects produce "lattice invariant deformation" (LID) in the nomenclature of the PTMC.

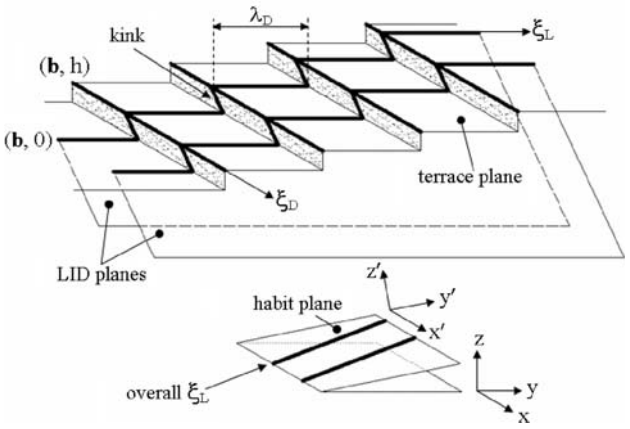

Fig. 1 Schematic illustration of a parent–martensite interface showing the terrace segments and defect arrays. Coherently strained terraces are reticulated by arrays of disconnections (**b**, h) with spacing λ_D and crystal slip or twinning dislocations (**b**, 0) in the (lower) martensite crystal. The terrace and habit (primed) coordinate frames are shown and the line directions of the disconnections, $\boldsymbol{\xi}_D$, and dislocations, $\boldsymbol{\xi}_L$, are parallel to x and close to y, respectively

The coherency distortion can be removed by superimposing an array of defects on the terraces, as in Fig. 1. Thus, the terraces remain coherent between the defects, and the distortion diminishes with distance from the interface, although a small rigid relative rotation of the phases may arise as a corollary as discussed further below. The orientation and spacing of the disconnections, $\boldsymbol{\xi}_D$ and λ_D, and LID, $\boldsymbol{\xi}_L$ and λ_L, can be found using the Frank-Bilby formalism [18]. In general, an iterative procedure is needed to obtain the equilibrium interface structure [19]; its orientation, the habit plane, is determined principally by ξ_D and λ_D, as in Fig. 1. In seeking an initial solution, $\boldsymbol{\xi}_D$ and $\boldsymbol{\xi}_L$ are allowed to have any orientation in the interface. This is not a restrictive condition for the disconnections since they are glissile. In general, the LID is expected to be oriented along the intersection of the glide/twinning plane with the habit plane, $\boldsymbol{\xi}_I$. If $\boldsymbol{\xi}_I$ and $\boldsymbol{\xi}_L$ differ by a small amount, the strain matrix with the latter orientation imposed can be calculated to estimate the residual strain energy. Of course glide dislocations with **b** parallel to the terrace plane can reorient by interface glide. Also, closely spaced or intersecting sessile LID dislocations can interact and move short distances by athermal climb. The relative orientation of the adjacent crystals and the transformation displacement can also be obtained [7].

Comparison of the phenomenological and topological models

The centrepiece of the PTMC is that the habit plane is an "undistorted and unrotated" plane of the shape deformation [20]. Although LID is invoked, it is modelled as a homogeneous deformation of the martensite, and the latter crystal is rigidly rotated to fit onto the fixed parent at the contact plane. By contrast, the TM envisions a coherent interface, reticulated by a network comprising an array of glissile disconnections and a second array of LID. For an ideal habit plane, the coherency distortions are removed at long range, although a rotation of each crystal way from the reference orientation may arise. However, in the immediate vicinity of the interface, the coherent reference configuration persists, and the defects accommodating the strains have topological parameters defined in that reference state. This near-distortion field predicted by the TM is important since it not only relates to the interfacial energy, but also to the mechanism of transformation and hence kinetics. The far-distortion field (rotation) predicted by the TM also leads to important differences from the PTMC; first, a small but systematic difference in predicted habit

plane arises, even when other crystallographic parameters are essentially identical, illustrated below by the β to α transformation in Ti. The second is that the TM predicts habit planes that are not invariant planes, and the {575} case of ferrous alloys is chosen as an example.

The β to α transformation in Ti

A feasible terrace structure for Ti is shown in Fig. 2; the strains necessary to bring the $(1\bar{1}00)_\alpha$ and $(2\bar{1}\bar{1})_\beta$ terraces into coherence, e_{xx} and e_{yy}, are indicated; to first order, the principal coherency strains are $\varepsilon_{xx} = 2e_{xx}$ and $\varepsilon_{yy} = 2e_{yy}$; we note that the signs of e_{xx} and e_{yy} are negative here corresponding to compression of α with respect to β. Formally, the coherency strain in the terrace with respect to the natural crystals, ${}_n\mathbf{E}_c$, is defined by

$$ {}_n\mathbf{E}_c = \begin{pmatrix} \varepsilon_{xx} & 0 & 0 \\ 0 & \varepsilon_{yy} & 0 \\ 0 & 0 & 0 \end{pmatrix}. \quad (1) $$

The total dislocation content needed to accommodate this strain, **B**, is given by the Frank-Bilby equation,

$$ \mathbf{B} = -{}_n\mathbf{E}_c\mathbf{v}, \quad (2) $$

where **v** is a probe vector in the interface. Eligible disconnections (**b**, h) and LID, (**b**, 0) can be determined from the dichromatic pattern [16]; a candidate disconnection is shown in Fig. 3, and the LID is known to be $(1\bar{1}01)_\alpha$ twinning which intersects the terrace plane along y [21]. Since the disconnections have step character, **v** cannot be defined precisely at this stage; initially, the step character is suppressed, so a provisional defect network is identified in the terrace plane. The

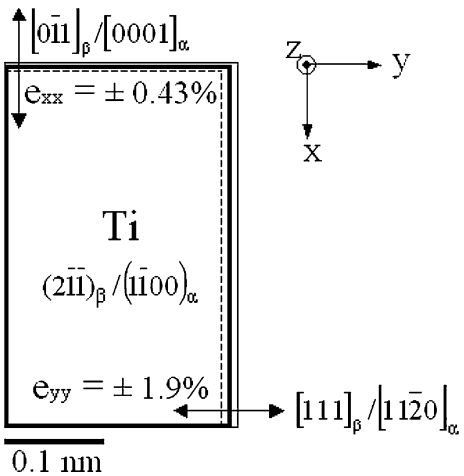

Fig. 2 Scale drawing of the terrace plane in Ti. Full lines represent the martensite and dashed lines the parent crystal, and bold lines depict the coherent state after equal and opposite straining, e_{xx} and e_{yy}, of each phase

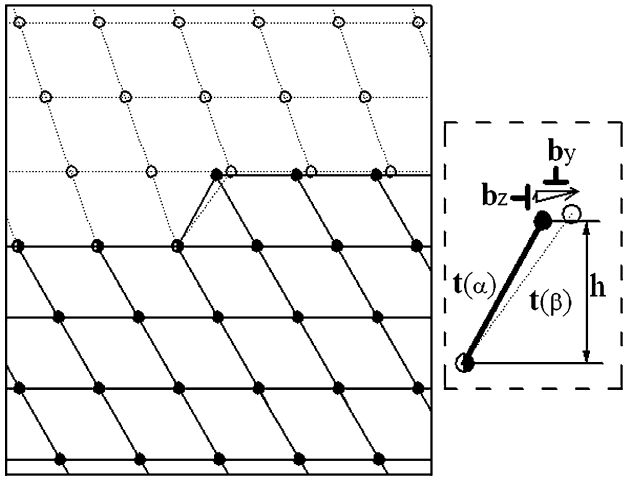

Fig. 3 Schematic illustration of the formation of a disconnection; the **b** of the defect with respect to the coherent reference state is the Volterra operation required to create equivalent interfaces on either side of the crystals' surface steps. The 'overlap' step height of the defect is the smaller of the two surface steps, h(α) in this case. The sense vector $\boldsymbol{\xi}$ points out of the page

normal components, b_z, of the Burgers vectors of the disconnections and dislocations are also suppressed; these components contribute additional small rigid-body rotations, φ_D and φ_L about $\boldsymbol{\xi}_D$ and $\boldsymbol{\xi}_L$, respectively, which can be superimposed separately. Using the current values of $\boldsymbol{\xi}_D$ and λ_D, one identifies an updated habit plane (primed coordinates in Fig. 1), and so on iteratively towards the equilibrium configuration. For simplicity in the present context, we ignore the small strain ε_{xx}, so that a simple disconnection network with **b** as in Fig. 3 and $\boldsymbol{\xi}_D$ parallel to x accommodates the misfit, Fig. 4. It has been shown elsewhere [6] that the equilibrium habit plane is inclined to the terrace plane by the angle θ, obtained from

$$ -\varepsilon_{yy} = \left(b_y \tan\theta + b_z \tan^2\theta\right)h^{-1}, \quad (3) $$

and φ_D is equal to

$$ \varphi_D = 2\sin^{-1}\left[\left(b_z\cos\theta - b_y\sin\theta - \varepsilon_{yy}h\cos\theta\right)\sin\theta/2h\right]. \quad (4) $$

For Ti, $\theta = 10.86°$, as depicted schematically in Fig. 5, which is close to the PTMC solution, $\omega = 11.36°$, depicted in Fig. 6. In this case φ_D is 0.528° for both the TM, expression (4), and the PTMC (see Fig. 6). Note that this value of φ_D is virtually equal to the apparent discrepancy $\omega - \theta$. This arises because the PTMC rotation is assumed to occur entirely in the martensite, Fig. 6. However, dislocation theory [22, 23] shows that the rotation φ_D, due to the normal components b_z' in Fig. 5, is partitioned between the two crystals, equally for an interface between isotropic materials of the same stiffness. As illustrated in Fig. 7, the TM model predicts that the apparent habit plane

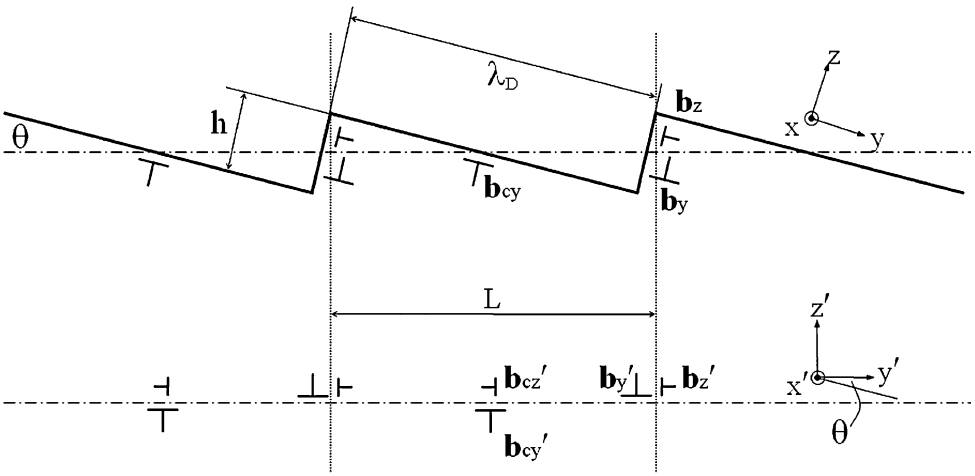

Fig. 4 Schematic illustration showing the disconnection content of a parent–martensite interface, with Burgers vector components resolved in the terrace (upper) and habit plane (lower) frames. The terrace plane is inclined at an angle θ to the horizontal habit plane. Coherency strain is represented by an equivalent defect content, $\mathbf{b}_c$

inclination for an observer in the parent remote from the interface, unable to resolve the near-field distortion (or an experimentalist using optical microscopy and X-ray diffraction), is $\theta + \varphi_D/2$, and, conversely, for an observer in the martensite, $\theta - \varphi_D/2$.

For a complete treatment, the accommodation of ε_{xx} must also be taken into account. The interested reader should see reference [7] where it is shown that twinning dislocations with $\boldsymbol{\xi}_L$ close to y, $\boldsymbol{b}$ parallel to $[1\bar{1}02]_\alpha$ and $\lambda_L = 7.16$ nm accommodate this strain, and introduce a rigid-body rotation φ_L equal to 0.263°. (For simplicity in analysis, the twinning dislocations are assumed to form an array of individual defects rather than coalescing into twins; the results for the two cases are the same except for some differences between the near-field distortions.)

The foregoing shows that the TM and PTMC solutions are very similar in the Ti case. In other words, the invariant

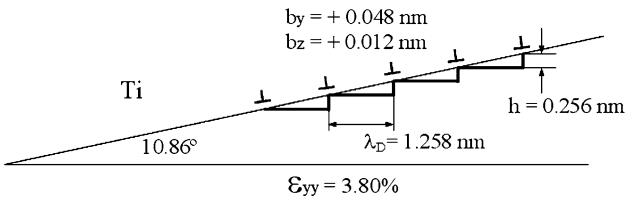

Fig. 5 Schematic illustration of the terrace/disconnection structure of the habit planes in Ti. The Burgers vector components of the disconnections, their step heights and the coherency strains are shown

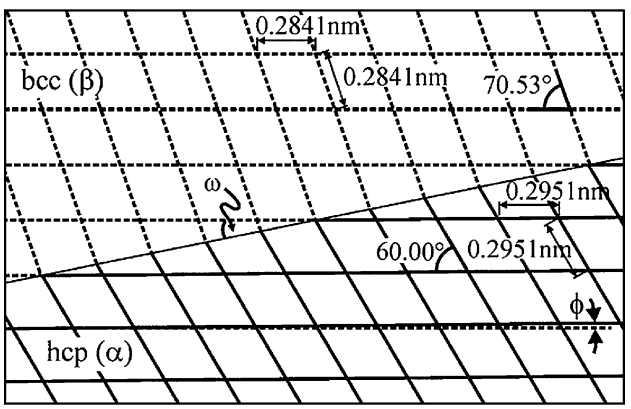

Fig. 6 Schematic illustration of parent and product lattices viewed along x for Ti assuming coherency normal to the page according to the PTMC

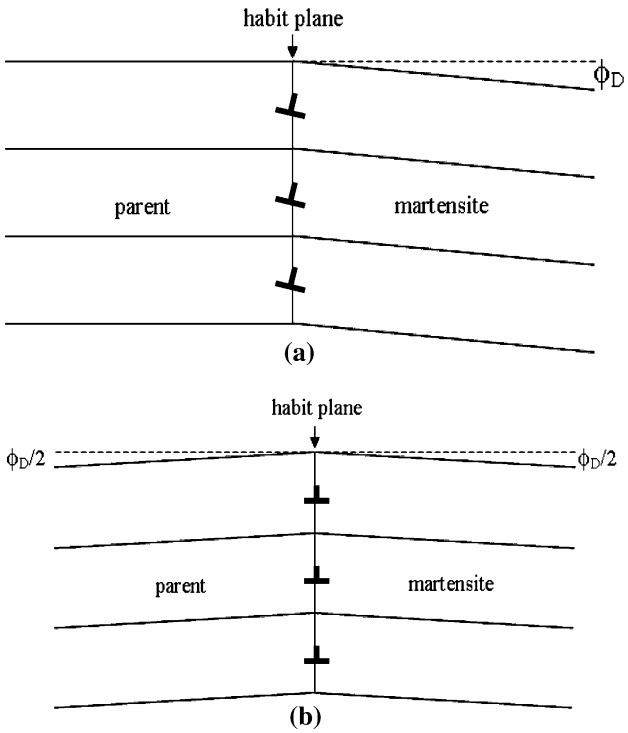

Fig. 7 Schematic illustration of the rotation φ_D (**a**) unpartitioned (PTMC), and (**b**) equally partitioned (TM); dislocation symbols represent the resultant Burgers vector content normal to the habit plane, b'_z, producing φ_D. The apparent inclination of the habit plane for observers in the parent and martensite, respectively, are (**a**) ω and $\omega - \varphi_D$, and (**b**) $\theta + \varphi_D/2$ and $\theta - \varphi_D/2$

plane concept of the PTMC is approximately valid macroscopically, and the TM provides additional details of the near-field distortion and slight modification of the apparent habit plane.

The γ to α transformation in ferrous alloys

A feasible terrace in this system is $(111)_\gamma/(011)_\alpha$; the principal strains of the natural crystals in the Nishyama-Wassermann (NW) orientation relationship to the coherent state are large, as illustrated in Fig. 8. Moreover, there is a multiplicity of plausible glissile disconnections and $1/2 < 111 >$ LID dislocations, as summarised in Table 1. Note that the Burgers vector of the disconnection designated $\mathbf{b}_{+1/+1}$ (i.e. with h = +1 in units of terrace plane spacing) is parallel to ε_{yy}, similarly to the case for Ti above. However, the Table shows that the b_x and b_y components of $\mathbf{b}_{-1/-1}$ disconnections, illustrated in Fig. 9, are both finite. Therefore, we explore semi-coherent interfaces based on $\mathbf{b}_{-1/-1}$ disconnections and $\mathbf{b}^{(i)}$ LID dislocations (derived from $\frac{1}{2}[1\bar{1}1]_\alpha$).

Consider the first stage of solving the Frank-Bilby equation, i.e. with normal components of $\mathbf{b}$ and steps

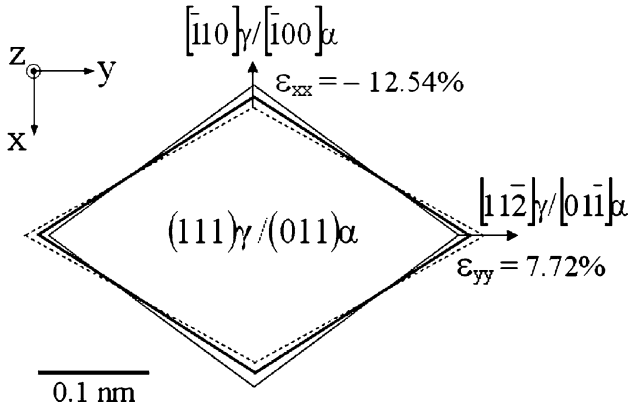

Fig. 8 Scale drawing of the atomic rhombi in the terrace plane of a ferrous alloy. Full lines represent the unstrained martensite, dashed lines the unstrained parent crystal and bold lines the coherent state

Table 1 Topological parameters of interfacial defects

	b_x (nm)	b_y (nm)	b_z (nm)	h^a	$\mathbf{t}(\gamma)$	$\mathbf{t}(\alpha)$
$\mathbf{b}^{(i)}$	0.135	−0.211	0	0	–	$\frac{1}{2}[1\bar{1}1]_\alpha$
$\mathbf{b}^{(ii)}$	−0.135	−0.211	0	0	–	$\frac{1}{2}[\bar{1}\bar{1}1]_\alpha$
$\mathbf{b}_{-1/-1}$	−0.135	−0.141	−0.004	−1	$\frac{1}{2}[\bar{1}\bar{1}0]_\gamma$	$\frac{1}{2}[1\bar{1}\bar{1}]_\alpha$
$\mathbf{b}_{-2/-2}$	−0.135	−0.070	−0.008	−2	$\frac{1}{2}[\bar{2}\bar{1}\bar{1}]_\gamma$	$[0\bar{1}\bar{1}]_\alpha$
$\mathbf{b}_{+1/+1}$	0	0.070	0.004	+1	$\frac{1}{2}[011]_\gamma$	$\frac{1}{2}[\bar{1}11]_\alpha$

[a] The "overlap" step height, h, is defined as the smaller of the terrace plane spacings, i.e. $(011)_\alpha$ in the present case

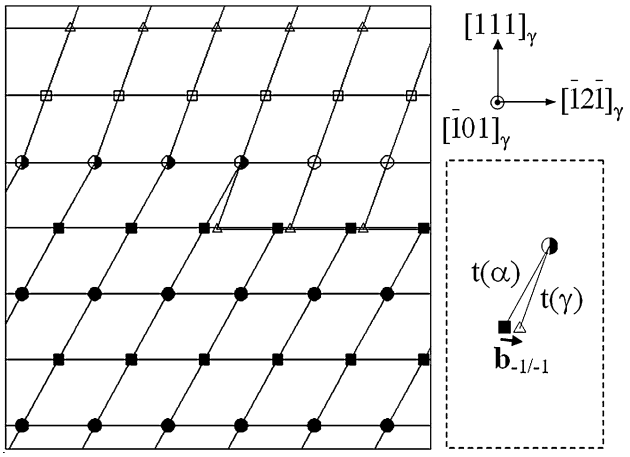

Fig. 9 Schematic illustration of a $\mathbf{b}_{-1/-1}$ disconnection in the coherent reference interface viewed along $[\bar{1}01]_\gamma/[\bar{1}\bar{1}1]_\alpha$. Lateral motion of such defects would cause transformation in a conservative manner. The symbols represent site levels along $[111]_\gamma$ /$[011]_\alpha$; note the large screw component when the defect is oriented along the viewing direction

suppressed. Let $\boldsymbol{\xi}_D$ and $\boldsymbol{\xi}_L$ subtend the angles χ_D and χ_L from the positive x-axis. Now choose a probe vector $\mathbf{v}_D$ parallel or (anti-parallel) to $\boldsymbol{\xi}_D$, such that it intersects only LID, and, similarly, $\mathbf{v}_L$ parallel or (anti-parallel) to $\boldsymbol{\xi}_L$ intersecting only disconnections. Thus, in the former case, the Burgers vector cut per unit length, $\mathbf{B}_L$, can be written as

$$\mathbf{B}_L = \frac{\mathbf{b}_L \sin(\chi_D - \chi_L)}{\lambda_L}, \tag{5a}$$

and, similarly,

$$\mathbf{B}_D = \frac{\mathbf{b}_D \sin(\chi_D - \chi_L)}{\lambda_D}. \tag{5b}$$

Equation (2) can now be expressed as

$$\mathbf{v}_D = \xi_D = (-_n\mathbf{E}_c)^{-1}\mathbf{B}_L, \tag{6}$$

and similarly for $\mathbf{v}_L$. Thus, the directions of $\mathbf{v}_D$ and $\mathbf{v}_L$ can be determined, hence giving the unit vectors $\boldsymbol{\xi}_D$ and $\boldsymbol{\xi}_L$ (from which χ_D and χ_L are found) and the separations λ_D and λ_L. The resulting network is shown in Fig. 10(a); the disconnections are close to screw orientation, as depicted in Fig. 9, and the LID is also very close to screw orientation. Mechanistically, these LID dislocations are supposed to glide into the interface as pure screw dislocations, so some interface glide rearrangement is needed for them to assume mixed orientation. Such near-screw configurations accommodating misfit were discussed by Matthews [24] who pointed out that additional twist misorientation has the effect of decreasing the spacing, λ, of one array and increasing the other and modifying $\boldsymbol{\xi}$ for both. Equation (6) is then modified, for small twists, and becomes

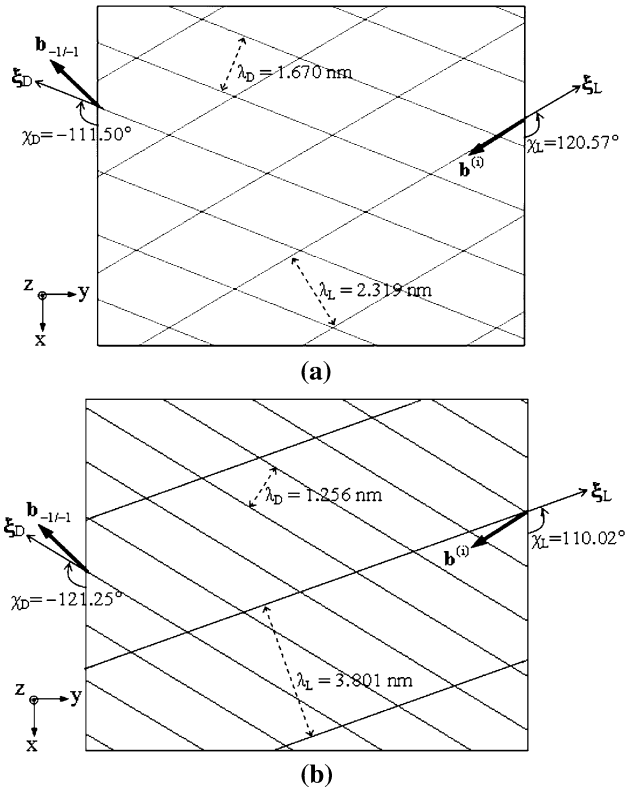

Fig. 10 Schematic illustration of defect networks with $\mathbf{b}^{(i)}$ LID and $\mathbf{b}_{-1/-1}$ disconnections for (**a**) $\tau = 0°$ and (**b**) $\tau = 2.5°$

$$\mathbf{v}_D = \xi_D = (-_n\mathbf{E}_c + \mathbf{R})^{-1}\mathbf{B}_L, \tag{7}$$

where $\mathbf{R} = \mathbf{R}^+ + \mathbf{R}^-.\mathbf{R}^+$ represents a rotation of γ by $+\tau/2$, and $\mathbf{R}^-$ is a rotation of α by $-\tau/2$ about the terrace normal, implying that this additional twist, like the tilts φ, is partitioned between the crystals. The network parameters, ξ_D, ξ_L, χ_D and χ_L for incremental twist deviation, τ, from the NW to the Kurdjumov-Sachs (KS) orientation, where $[\bar{1}01]_\gamma$ is parallel to $[\bar{1}\bar{1}1]_\alpha$ [25], i.e. $\tau = 0°$ to 5.26°, are listed in Table 2, and a schematic illustration of the network for $\tau = 2.5°$ is shown in Fig. 10(b).

Table 2 Network parameters for $\mathbf{b}^{(i)}$ LID and $\mathbf{b}_{-1/-1}$ disconnections.

τ (°)	χ_L (°)	λ_L (nm)	χ_D (°)	λ_D (nm)	ψ (°)
0	120.57	2.319	−111.50	1.670	6.93
0.5	119.18	2.520	−113.93	1.571	7.36
1.0	117.53	2.757	−116.08	1.481	7.80
1.5	115.53	3.039	−118.00	1.399	8.26
2.0	113.08	3.381	−119.71	1.324	8.72
2.5	110.02	3.801	−121.25	1.256	9.18
3.0	106.10	4.320	−122.64	1.193	9.65
3.5	100.98	4.969	−123.89	1.137	10.12
4.0	94.13	5.775	−125.03	1.084	10.60
4.5	84.82	6.736	−126.07	1.037	11.08
5.0	72.30	7.745	−127.03	0.992	11.56
5.26	64.27	8.200	−127.50	0.971	11.81

The next stage of iterations for the solutions described above is to introduce the step character of the disconnections and hence define the provisional habit plane. The normal to this plane is determined by rotating the normal to the terrace plane by the angle $\psi = \tan^{-1}\frac{h}{\lambda_D}$ about an axis parallel to ξ_D and the values so obtained are included in Table 2. The habit plane for the configuration depicted in Fig. 10(b), expressed in the parent crystal frame, is (0.505 0.700 0.505)$_\gamma$. Further refinement would require the b_z components of the disconnections to be reinstated and the defect content on the habit plane re-determined using probe vectors in that plane. At equilibrium, the misfit along this plane must be accommodated by the defect network, and further adjustments of defect line directions and separations may be needed. Defect content with resultant component of **B** perpendicular to the final habit plane does not affect misfit-relief; it acts as a low-angle tilt boundary thereby introducing an ancillary change in φ.

The TM applied to this case gives a range of possible habit plane solutions, in contradistinction to the invariant plane notion. The key structural difference between this Fe and the Ti case is that here the components of $\mathbf{b}_{-1/-1}$ and $\mathbf{b}^{(i)}$ parallel to the terrace plane are not aligned with the principal strains. Consequently, a network of near screw defects accommodates the misfit, and additional twist can be superimposed. The interfacial energy will vary with increasing twist and may be minimal for some finite value. A further consideration is the deviation between ξ_L and ξ_I for a particular solution; additional strain energy will arise if the LID cannot reorient in the habit plane ($\xi_L = \xi_I$). On the other hand, significant deviation of ξ_L from ξ_I would cause the LID to become sessile with respect to motion normal to the terrace plane, possibly retarding disconnection motion.

Although the habit plane structures reported here are not fully refined, the provisional structures show good agreement with experimental observations in the literature. For example, Sandvik and Wayman [26] and Kelly et al. [27] studied lath martensite in an FeNiMn alloy using transmission electron microscopy (TEM). They observed an array of $\frac{1}{2}[1\bar{1}1]_\alpha$ LID dislocations with λ_L in the range 2.6–6.3 nm, ξ_L varying between 10° and 15° from screw orientation in a habit plane with $\psi = 9.45°$, and τ ranging between 0.16° and 3.16°. This observation resembles closely the array of $\mathbf{b}^{(i)}$ and $\mathbf{b}_{-1/-1}$ defects predicted here (Table 2 and Fig. 10(b)) for $\tau = 2.5°$, namely: $\lambda_L = 3.77$ nm, ξ_L oriented 12.99° from screw orientation and habit plane very close to (575). Reinstating the small components of b_z for the $\mathbf{b}^{(i)}$ and $\mathbf{b}_{-1/-1}$ defects produces additional tilts, φ_L and φ_D, about ξ_L and ξ_D, respectively, where $\varphi_L = \sim -0.54°$ and $\varphi_D = \sim 0.14°$ in this case; these contributions slightly modify the

relative orientation , misaligning the $(111)_\gamma$ and $(011)_\alpha$ planes for example.

Discussion

The TM has been used here to find the interfacial structure of habit planes between parent and martensite phases; so called "single interface" habit planes are considered, i.e. where normal strains are able to relax. The predicted interfaces are glissile and exhibit no long-range distortion field except for ancillary tilt and twist rotations away from the reference orientation relationship. Near-field distortions accommodate the coherent terraces to the adjacent unstrained crystals. Coherency is essential for the transformation mechanism to occur in a military manner without long-range diffusion.

The energy per unit length of an array of dislocations, $\frac{W}{L}$, has the form

$$\frac{W}{L} = \frac{A}{\lambda}\left[b_s^2 \ln\frac{\lambda}{C_s} + \frac{b_e^2}{(1-\nu)} \ln\frac{\lambda}{C_e}\right], \quad (8)$$

where the subscripts s and e stand for screw and edge, respectively, C is the core parameter and υ is Poisson's ratio. According to simulations as well as the Peierls model [22] the core energy is larger for screws, i.e. $C_s < C_e$ so, for large λ, Eq. (8) indicates that screw arrays have a smaller line tension than the edges. However, for small λ the core parameter can dominate and the edges can have smaller line tension than screws. Since $\varepsilon \propto \frac{b}{\lambda}$, expression (8) also shows that $\frac{W}{L} \propto b$, implying that defects with smaller Burgers vectors accommodate coherency strain more efficiently.

The overall energy comprises the dislocation energies of the disconnection and LID arrays, their interaction energy, a contribution from the disconnections' step risers and the interfacial free energy of the terrace segments. Both the disconnections and the LID dislocations have some spreading width, so the coherent area decreases as λ decreases. In the limit $\lambda \to$ b, the interface becomes incoherent with higher energy.

In the case of Ti, the predicted interface crystallography is very similar to the solution obtained using the PTMC, apart from a small difference of habit due to partitioning of ancillary tilts. In this case the major part of the interfacial coherency strain is relieved by the disconnections and the strain (3.8%) is small enough that elastic energy should dominate in Eq. (8). Thus, the LID defects have a minor contribution to the energy of the interface. Hence one expects an array of edge disconnections with the minimum possible $b = b_e$ that still permits the terraces to be coherent, so that they have relatively low interfacial energy. More deformation systems could be added, provided that the net **B** is the same, but that would decrease the coherent area and hence increase the energy. Experiment agrees with this expectation of disconnections in edge orientation, although the step height is twice that of a single disconnection [28]. We speculate that this increases the area of coherent terrace, offsetting the attendant increase in elastic energy.

The ferrous case is more complex because the coherency strains are larger. An orthogonal array analogous to the Ti case is possible. An array of $\mathbf{b}_{+1/+1}$ disconnections could efficiently accommodate ε_{yy} and introduce only a small tilt ϕ_D (see Table 1 for components of $\mathbf{b}_{+1/+1}$). However, there is no suitable single mode of LID to accommodate ε_{xx}. One possible solution would be to activate two slip systems, producing an array of alternating $\mathbf{b}^{(i)}$ and $-\mathbf{b}^{(ii)}$ dislocations parallel to y. The b_y components are effectively cancelled, but, since these are relatively large (Table 1), there is a significant increase in the array's energy. On the other hand, the network shown in Fig. 10(a), $\mathbf{b}^{(i)}$ and $\mathbf{b}_{-1/-1}$ defects with $\tau = 0°$, is thought to be favourable, although the total energy has not been estimated. The network with $\tau = 2.5°$ corresponding to a {575} habit shown in Fig. 10(b) may have still lower energy. As described above, experimental observations of this interface are in good agreement with the predicted network. Thus, in the case of Fe alloys we have demonstrated that significant differences can arise between the TM and PTMC; in particular, the instance of {575} habits, which cannot be explained satisfactorily using a single mode of LID in the PTMC framework [5], is addressed. According to the TM, this habit is not an invariant plane of the shape transformation, which explains why the PTMC is not applicable in this case. The predicted defect network comprises near-screw disconnections and dislocations, in contrast to arrays of edge defects which are more familiar agents of misfit accommodation.

It is beyond the scope of this article, but there is another factor that can be important for plates with small aspect ratios, i.e. relatively small λ values. In such plates rotations accompanying both disconnection and LID motion produce incompatibilities at plate edges, with accompanying elastic or plastic strain. This factor may favour the activation of multiple LID systems to minimise rotation for both disconnections and LID. The von Mises criterion applies, so no more than five independent systems among disconnections and LID are required in the most general case. There is evidence from nano-rolled Nb–Cu layered structures that the four glide, symmetric slip, no rotation KS mechanism can operate up to very large strains, so it is also feasible as a LID type for the much lower ($\sim$10% vs. $\sim$300%) strains in the martensite case [29].

References

1. Christian JW (2002) The theory of transformations in metals and alloys. Pergamon Press, Oxford
2. Olson GB, Owen WS (eds) (1992) Martensite. ASM International, USA
3. Wechsler MS, Lieberman DS, Read TA (1953) Trans AIME 197:1503
4. Bowles JS, MacKenzie JK (1954) Acta Metall 2:129, 138, 224
5. McDougall PG, Wayman CM (1992) In: Olson GB, Owen WS (eds) Martensite. ASM International, USA, p 59
6. Pond RC, Celotto S, Hirth JP (2003) Acta Mater 51:5385
7. Pond RC, Hirth JP, Ma X, Chai YW (2007) Topological modelling of martensitic transformations. In: Nabarro FRN, Hirth JP (eds) Dislocations in solids, vol. 13. Elsevier, Amsterdam, p 227
8. Hirth JP (1994) J Phys Chem Sol 55:985
9. Sutton AP, Balluffi RW (1995) Interfaces in crystalline materials. Clarendon Press, Oxford
10. Hall MG, Aaronson HI, Kinsman KR (1972) Surf Sci. 31:257
11. Roitburd AL (1976) Solid State Phys 33:317
12. Dahmen U (1987) Scripta Metall 21:1029
13. Smith DA (1987) Scripta Metall 21:1009
14. Pond RC, Ma X (2005) Z fur Metal 96:1124
15. Crocker AG (1962) Philos Mag 7:1901
16. Pond RC (1989) Line defects in interfaces. In: Nabarro FRN (ed) Dislocations in solids, vol. 8. North-Holland, Amsterdam, p 1
17. Christian JW (1994) Metall Mater Trans 25A:1821
18. Bilby BA, Bullough R, Smith E (1955) Proc Roy Soc 231A:263
19. Ma X, Pond RC (2007) J Nucl Mater 361:313
20. Wayman CM (1964) Introduction to the crystallography of martensite transformations. Macmillan, New York
21. Hammond C, Kelly PM (1969) Acta Metall 17:869
22. Hirth JP, Lothe J (1982) Theory of dislocations. McGraw-Hill, New York
23. Hirth JP, Pond RC, Lothe J (2006) Acta Mater 54:4237–4245
24. Matthews JW (1974) Phil Mag 29:797
25. Kurdjumov GV, Sachs G (1930) Z Phys 64:325
26. Sandvik BPJ, Wayman CM (1983) Metall Trans 14A:835
27. Kelly PM, Jostsons A, Blake RG (1990) Acta Metal Mater 38:1075
28. Pond RC, Celotto S (2003) Int Mater Rev 48:225
29. Misra A, Hirth JP, Hoagland RG, Embury JD, Kung H (2004) Acta Mater 52:2387